Available online at www.sciencedirect.com
ScienceDirect
International Journal of Heat and Mass Transfer 50 (2007) 789–798
International Journal of HEAT and MASS TRANSFER
www.elsevier.com/locate/ijhmt

A semi-analytical method to study the temperature evolutions of a slab and a semi-infinite target for plasma immersion ion implantation

F.B. Yeh *

Department of Marine Mechanical Engineering, Chinese Naval Academy, P.O. Box 90175, Tsoying, 813, Kaohsiung, Taiwan, ROC

Received 25 January 2006; received in revised form 22 August 2006
Available online 23 October 2006

Abstract

The problems of heating a slab of finite thickness and a semi-infinite target with repetitive high negative bias voltage pulses in contact with a plasma are solved by using the two-dimensional Laplace integral transform technique. The plasma is composed of a collisionless presheath and sheath on an electrically negative biased wall, which partially reflects and secondarily emits ions and electrons. The heating of the workpiece from the plasma accounting for the presheath and sheath is determined by kinetic analysis. This work proposes a semi-analytical model to calculate the temperature evolutions and the melting times of the front surface of a slab and a semi-infinite target, and provides quantitative results applicable to control the temperature evolutions and the melting times. The predicted surface temperature of the slab as a function of time is found to agree well with experimental data. The effects of dimensionless pulse parameters, including the pulse duty cycle and pulse bias voltage, on the melting time and heating rate of the front surface are obtained. The results show that the temperatures and heating rates of the front surface of the slab and target increase with pulse parameters. The melting times to initiate the melting at the front surface are strongly dependent on the pulse parameters. The heat flux transport to workpiece from plasma is important to increase the surface temperature of the workpiece when the bias voltage is switched-off for low pulse duty cycle and low pulse bias voltage. The temperature of the workpiece is underestimated when not accounting for the heating effects during the pulse-off duration for low value of pulse parameters.

Keywords: Plasma energy flux; Pulse duty cycle; Pulse bias voltage; Laplace integral transform

1. Introduction

Plasma immersion ion implantation (PIII) technique is an advanced surface modification method to increase the hardness, wear, and corrosion resistance of the surface of materials. Except for metallurgical engineering, PIII excels in semiconductor and microelectronics processing as well as biomedical engineering. It has been used to dope shallow junctions, synthesize silicon-on-insulator (SOI) structures, process flat panel display materials, deposit thin film and so on [1]. The PIII technology has many advantages over conventional implantation, such as high dose rates, wide ion energy range, large implant areas and treatment of complex shapes. The process is performed by repetitively applying a large negative-voltage pulse to a substrate immersed in a plasma that was initially developed by Conrad et al. [2,3] in 1987. A high negative-voltage pulse is applied to the substrate during the pulse-on duration, electrons near the substrate are driven away within the time scale of the inverse electron plasma frequency and ions to be accelerated implanting into the near surface of substrate are extracted directly from the plasma in the time scale of the inverse ion-plasma frequency. During the pulse-off duration, the density flux of electrons is just equal to the density flux of ions reaching the substrate and the substrate is self-bias (floating voltage). In PIII, an ion sheath conformably surrounding the substrate is formed, all surface are implanted at the same time, leading to significantly reduced implantation times and cost-effective implantation.

* Tel./fax: +886 7 5834861.
E-mail address: fbyeh@mail.cna.edu.tw

0017-9310/$ - see front matter © 2006 Elsevier Ltd. All rights reserved.
doi:10.1016/j.ijheatmasstransfer.2006.08.019

Nomenclature

Bi	Biot number, $Bi = h_\infty s/k$
c_p	specific heat
e	electron charge
E_i	dimensional and dimensionless ionization energy, $E_i = E_i/k_B T_{e0}$
f	pulse frequency, $f = 1/(\tau_{on} + \tau_{off})$
h	heat transfer coefficient
j	dimensional and dimensionless current density, $j = j/en_{e0}(K_B T_{e0}/m_i)^{1/2}$
k	solid thermal conductivity
k_B	Boltzmann constant
m	particle mass
M	ion-to-electron mass ratio, $M = m_i/m_e$
n	particle density
P	the repetitive pulses function, defined in Eq. (7)
Q	dimensional and dimensionless total energy flux, $Q = Q/[n_{eo}k_B T_{e0}(k_B T_{e0}/m_i)^{1/2}]$
s	the thickness of slab
t	time
T	temperature
x	Cartesian coordinate
Z_i	ion charge number

Greek symbols

Θ	plasma flow work-to-thermal conduction ratio, $\Theta = n_{e0}k_B T_{e0}(k_B T_{e0}/m_i)^{1/2}/(kT_\infty/s)$
λ	dimensionless temperature, $\lambda = (T - T_\infty)/T_\infty$
ξ	dimensionless coordinate, $\xi = x/s$
φ	dimensional and dimensionless work function, $\varphi = \varphi/k_B T_{e0}$
γ	ion and electron reflectivity
κ	electron-to-ion source temperature ratio at the presheath edge, $\kappa = T_{e0}/T_{i0}$
ρ	density
δ	pulse duty cycle, $\delta = \tau_{on}/(\tau_{on} + \tau_{off})$
η	pulse efficiency, $\eta = \lambda_{on}/\lambda$
τ	dimensionless time, $\tau = kt/\rho c_p s^2$
ϕ, χ	dimensional and dimensionless potential, $\chi = -e\phi/k_B T_{e0}$
Δ_1, Δ_2	functions, defined in Eqs. (5) and (6)
Ω, Ω_{1b}	functions, defined in [5,24]

Subscripts

b	boundary between sheath and presheath
bias	negative bias voltage
e, i	electron and ion
m	melting
off	pulse-off duration
on	pulse-on duration
s	slab
t	semi-infinite target
w	wall
∞	ambient
o, o′	coordinate origin at $\phi = 0$ and $\xi = 0$, respectively, as shown in Fig. 1(a) and (b)

Fundamental to understand and model this process is the plasma–wall interaction that leads to an electrically charges sheath and neutral presheath between the wall and the plasma [4,5]. There are several published models for the dynamic plasma sheath, from analytical expressions [6–12] to kinetic simulations [13–15], including one which simulated the PIII for voltage pulse with finite rise and fall times [16].

One important parameter of the PIII process is the target temperature reached during the processing. High temperature is desirable in cases where diffusion of the implanted species is desired. On the other hand, high temperature is undesirable in many cases, such as for material which temper at relatively low temperature. Precise controlling of the substrate temperature is extremely important in PIII of semiconductors. For example, the silicon wafer temperature must be heated to 600 °C or higher in separation by plasma implantation of oxygen, and in the PIII/ion cut process, the wafer temperature must remain below 300 °C during implantation [17]. Many methods and models have been proposed for measurement and prediction of the substrate temperature in the plasma [17–23]. Tian et al. [17,18] proposed a thermocouple-based direct temperature measurement system to monitor the temperature evolution of silicon wafers during hydrogen plasma immersion ion implantation. Experimental results indicated that implantation voltage, pulse duration and pulse frequency affect strongly the substrate temperature. The substrate temperature rises linearly with the implantation time and the source of heating substrate is mainly from ions bombardment. Contrary to the temperature rise with respect to implantation voltage and pulse duration, the relationship between the temperature rise and pulse frequency is almost linear. In another work, a two-dimensional fluid model is proposed by Tian and Chu [19] to simulate the sheath dynamics including the ion distribution, sheath configuration, incident ion fluxes and energy imported to the substrate by the ions. The calculated heat input is used to predict the temperature rise of substrate with two-dimensional unsteady conduction equation. The simulation results indicate that the temperature gradients in target are very small for a small target in the high-frequency, low-voltage PIII process. Takaki et al. [20] developed a measurement method based on monitoring the variation of natural birefringence due to the changed temperature by interferometry, to measure the transient temperature rise of the substrate in a capacitively coupled RF plasma by varying the repetition rate of the negative bias pulse. The heat flux

increases with the repetition rate of the bias pulse is presented. Nitrogen ions are implanted into low carbon steel under various pulse bias voltages and nitrogen pressure that are investigated experimentally by Mitsuo et al. [21]. Experimental results showed that the temperature of the substrate is risen proportion to the pulse bias voltage and nitrogen-affected region became deeper with bias voltage and nitrogen pressure. A time dependent lumped capacity and cycle-averaged thermal model is developed by Blanchard [22] to predict target temperature in PIII by neglecting the temperature gradients in target. Manova et al. [23] measured the silicon target temperature using an IR pyrometer during PIII of nitrogen. The equilibrium repetition frequency for each given pulse bias voltage is determined by heating the target to the desired temperature. These results also present the depletion of the ions from the plasma during the pulses leads to reduced average plasma density at high repetition rates. The rise of surface temperature of the substrate results from the heating of plasma and ions, respectively, it corresponds to the pulse-off and pulse-on durations during a pulse cycle. In above-mentioned works, few researches study the heating effects from plasma for pulse-off duration during repetitive pulse cycles. The heat flux incident on the substrate and the substrate temperature are underestimated for low value of pulse parameters, which include the pulse duty cycle and pulse bias voltage, when the heat flux transport to the substrate from plasma during the pulse-off duration is ignored.

In this work, a one-dimensional semi-analytical model is proposed to simulate the temperature evolution of a workpiece when a repetitive high negative bias voltage is applied to the workpiece during PIII. For simplicity, the rise and fall times during a pulse cycle are neglected. Using this model, the effects of the pulse duty cycle and pulse bias voltage on the workpiece temperature can be determined. This work provides process designers to be able to predict the workpiece temperature for a wide variety of process parameters in PIII.

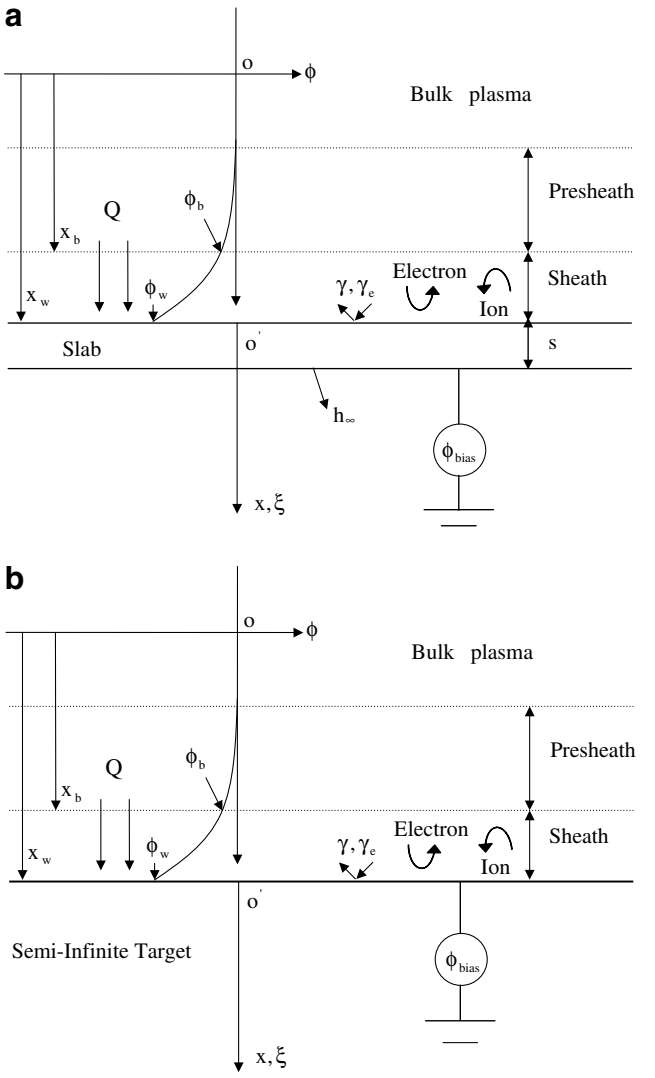

Fig. 1. Sketch for the physical model and coordinates: (a) a slab; and (b) a semi-infinite target.

2. Analytical model

In this study, a slab of finite thickness s and a semi-infinite target at room temperature T_0 are subjected to energy transport from plasma, as illustrated in Figs. 1(a) and (b), respectively. The plasma, comprised of the bulk plasma, presheath and sheath, is in contact with an electrically negative bias wall partially reflecting or secondarily emitting ions and electrons. When a series of high bias voltage pulse is applied to the slab and target, high energies of the ions perpendicularly to the front surface increase the temperature of the slab and target. Conduction is removed by convection at the bottom surface of the slab with heat transfer coefficient h_∞. The major assumptions made are as follows [4,5,24]:

1. The model is one-dimensional due to a thin thickness of the region considered.
2. The plasma energy flux incident on the front surface of the workpiece is considered as a surface heat source.
3. The plasma is in a quasi-steady state. The incident plasma irradiance on the front surface of the workpiece is function of time, while heat transfer in the slab and target is unsteady.
4. The transport processes in the plasma in contact with the workpiece surface can be modeled as those in the plasma between two parallel plates.
5. The workpiece surface is electrically biased.
6. The physical and thermal parameters of the slab are same as the semi-infinite target. Joule heat in the workpiece and the energy loss from thermal radiation are neglected.
7. The effects of pulse-rise and pulse-fall during a pulse cycle on the energy transport from plasma to workpiece surface are neglected. The repetitive pulses function is rectangular pulses.

2.1. Plasma energy transport to workpiece surface

The dimensionless plasma energy flux transport to the negative DC biased surface is given by [24]

$$Q = j_{iw}\left(\Omega + \chi_w - \chi_b + \frac{E_i}{Z_i} - \varphi\right) + j_{ew}(2+\varphi) \tag{1}$$

The ion and electron current densities at the wall in Eq. (1) are, respectively,

$$j_{iw} = \Omega_{1b} e^{-\chi_b}, \quad j_{ew} = (1-\gamma_e)\sqrt{\frac{M}{2\pi}} e^{-\chi_w} \tag{2}$$

where functions Ω and Ω_{1b} in Eqs. (1) and (2) are, respectively, defined in [5,24]. The dimensionless energies E_i and φ in Eq. (1) are referred to ionization energy and work function, respectively. The dimensionless sheath edge potential χ_b can be determined in [24]. Eq. (2) shows that ion current density at the wall is independent of the wall potential, while the electron current density rapidly decreases with increasing the wall potential. The wall potential is equal to the bias voltage and the floating potential during the pulse-on and pulse-off durations, respectively. The dimensionless wall potential yields [24]

$$\chi_w = \begin{cases} \chi_b + \ln\left(\frac{1-\gamma_e}{\Omega_{1b}}\sqrt{\frac{M}{2\pi}}\right), & \text{for } \chi_{bias} = 0, \\ \chi_{bias}, & \text{for } \chi_{bias} \gg 0 \end{cases} \tag{3}$$

where the dimensionless high bias voltage χ_{bias} is the magnitude of a repetitious pulse and larger than zero. The electron current density at the wall is reduced to zero during the pulse-on duration, $j_{ew} \to 0$ for $\chi_w \to \infty$. The dimensionless plasma energy flux transport to the repetitious pulse biased surface can be simplified to

$$Q(\tau) = j_{iw}[\Delta_1 + (\chi_{bias} - \Delta_2)P(\tau)] \tag{4}$$

with functions

$$\Delta_1 = \Omega + \ln\left(\frac{1-\gamma_e}{\Omega_{1b}}\sqrt{\frac{M}{2\pi}}\right) + \frac{E_i}{Z_i} + 2 \tag{5}$$

$$\Delta_2 = 2 + \varphi + \ln\left(\frac{1-\gamma_e}{\Omega_{1b}}\sqrt{\frac{M}{2\pi}}\right) + \chi_b \tag{6}$$

The repetitive pulses function (rectangular pulses) $P(\tau)$ is defined as

$$P(\tau) = \begin{cases} 1, & \text{for } \frac{n-1}{f} \leqslant \tau \leqslant \frac{n+\delta-1}{f}, \\ 0, & \text{for } \frac{n+\delta-1}{f} < \tau < \frac{n}{f}, \end{cases} \quad n = 1,2,3,4,\ldots \tag{7}$$

where τ denotes dimensionless time and is defined in later. The first term on the right hand side of Eq. (4) represents the plasma energy flux consisting of ion and electron energy flux, the front surface of the workpiece is electrically floating and the bias voltage pulse is switched-off, $P(\tau) = 0$. The second term on the right hand side of Eq. (4) represents the effects of repetitious pulses of bias voltage on the plasma energy flux, and the electron energy flux is zero when the bias voltage pulse is switched-on, $P(\tau) = 1$. The pulse frequency and pulse duty cycle are, respectively, defined as

$$f = \frac{1}{\tau_{on} + \tau_{off}}, \quad \delta = \frac{\tau_{on}}{\tau_{on} + \tau_{off}} \tag{8}$$

where τ_{on} and τ_{off} denote the dimensionless times for the pulse-on and pulse-off durations, respectively.

2.2. Plasma heating of a slab

The one-dimensional, unsteady heat conduction equation for the slab in dimensionless forms, yields

$$\frac{\partial \lambda_s(\xi,\tau)}{\partial \tau} = \frac{\partial^2 \lambda_s(\xi,\tau)}{\partial \xi^2} \tag{9}$$

The subscript s denotes the slab. The initial and boundary conditions for the slab are, respectively,

$$\lambda_s(\xi,0) = 0 \tag{10}$$

$$-\frac{\partial \lambda_s(0,\tau)}{\partial \xi} = \Theta Q(\tau) \tag{11}$$

$$-\frac{\partial \lambda_s(1,\tau)}{\partial \xi} = Bi\lambda_s(1,\tau) \tag{12}$$

where dimensionless parameter Θ represents the ratio between plasma flow work and heat conduction into the slab. Bi is Biot number. Taking the Laplace transform with respect to time and space coordinate, and using the initial and boundary conditions of Eqs. (10) and (11), the Eq. (9) can be expressed as

$$\tilde{\tilde{\lambda}}_s(p,s) = \frac{p}{p^2 - s}\tilde{\lambda}_s(0,s) - \Theta\frac{Q(s)}{p^2 - s} \tag{13}$$

where $\tilde{\tilde{\lambda}}_s(p,s)$is the Laplace transform of $\lambda_s(\xi,\tau)$ with respect to ξ and τ; $\tilde{\lambda}_s(0,s)$ is the Laplace transform of $\lambda_s(\xi,\tau)$ with respect to τ at $\xi = 0$; $Q(s)$ is the Laplace transform of $Q(\tau)$. The inverse Laplace transform with respect to p of the above equation gives

$$\tilde{\lambda}_s(\xi,s) = \tilde{\lambda}_s(0,s)\cosh(\sqrt{s}\xi) - \Theta\frac{Q(s)}{\sqrt{s}}\sinh(\sqrt{s}\xi) \tag{14}$$

Differentiating Eq. (14) with respect to ξ and substituting into boundary condition of Eq. (12), the quantity $\tilde{\lambda}_s(0,s)$ can be found as

$$\tilde{\lambda}_s(0,s) = \Theta Q(s)\frac{\sqrt{s}\cosh(\sqrt{s}) + Bi\sinh(\sqrt{s})}{s\times\sinh(\sqrt{s}) + Bi\sqrt{s}\cosh(\sqrt{s})} \tag{15}$$

Substituting the quantity back into Eq. (14), yields

$$\tilde{\lambda}_s(\xi,s) = \Theta Q(s)\left\{\frac{\sqrt{s}\cosh(\sqrt{s}(1-\xi)) + Bi\sinh(\sqrt{s}(1-\xi))}{s\times\sinh(\sqrt{s}) + Bi\sqrt{s}\cosh(\sqrt{s})}\right\} \tag{16}$$

To evaluate the inverse of this equation, the only poles needing consideration result from the equation

$$\coth(\sqrt{s}) = -\frac{\sqrt{s}}{Bi}, \quad \text{or} \quad \cot(i\sqrt{s}) = \frac{i\sqrt{s}}{Bi} \tag{17}$$

Let $\beta = \mathrm{i}\sqrt{s}$, it is necessary to determine the roots of the equation

$$\cot\beta = \frac{\beta}{Bi} \tag{18}$$

Differentiating the denominator of Eq. (16) with respect to s, yields

$$\frac{\mathrm{d}}{\mathrm{d}s}\left[s\times\sinh(\sqrt{s}) + Bi\sqrt{s}\cosh(\sqrt{s})\right] = \frac{1}{2\sqrt{s}}\left[(s+Bi)\cosh(\sqrt{s}) + (2\sqrt{s}+Bi\sqrt{s})\sinh(\sqrt{s})\right] \tag{19}$$

Expressing $\cosh(\sqrt{s})$ in terms of $-\sqrt{s}\sinh(\sqrt{s})/Bi$ from Eq. (17) and changing to trigonometric functions, yields

$$i\frac{\mathrm{d}}{\mathrm{d}s}\left[\mathrm{s}\times\sinh(\sqrt{s}) + Bi\sqrt{s}\cosh(\sqrt{s})\right] = \left(\frac{Bi^2+Bi+\beta^2}{2Bi}\right)\sin\beta \tag{20}$$

Applying the Heaviside expansion formula as

$$L^{-1}\left\{\frac{R(s)}{W(s)}\right\} = \sum_{k=1}^{n}\frac{R(\alpha_k)}{W'(\alpha_k)}\times \mathrm{e}^{\alpha_k\tau} \tag{21}$$

$R(s)$ and $W(s)$ are polynomials where $R(s)$ has degree less than that of $W(s)$. $W(s)$ has n distinct zeros α_k, $k = 1,2,3,\ldots,n$. Let

$$F(\xi,\tau) = L^{-1}\left\{\frac{\sqrt{s}\cosh(\sqrt{s}(1-\xi)) + Bi\sinh(\sqrt{s}(1-\xi))}{s\times\sinh(\sqrt{s}) + Bi\sqrt{s}\cosh(\sqrt{s})}\right\} = 2\sum_{n=1}^{\infty}\frac{(Bi^2+\beta_n^2)\cos\beta_n\xi}{(Bi^2+Bi+\beta_n^2)}\times\mathrm{e}^{-\beta_n^2\tau} \tag{22}$$

The variables of β_n are eigenvalues satisfied by $\beta_n\tan\beta_n = Bi$. The Laplace convolution $F(\xi,\tau) * Q(\tau)$ of $F(\xi,\tau)$ and $Q(\tau)$ is

$$L^{-1}\{F(\xi,s)Q(s)\} = F(\xi,\tau)*Q(\tau) = \int_0^{\tau}F(\xi,\tau-u)Q(u)\,\mathrm{d}u \tag{23}$$

The inverse Laplace transforms of the Eq. (16) can be expressed as

$$\lambda_{\mathrm{s}}(\xi,\tau) = 2\Theta j_{\mathrm{iw}}\left\{\Delta_1\times\sum_{n=1}^{\infty}\frac{(Bi^2+\beta_n^2)\cos\beta_n\xi}{\beta_n^2(Bi^2+Bi+\beta_n^2)}\times(1-\mathrm{e}^{-\beta_n^2\tau}) + (\chi_{\mathrm{bias}}-\Delta_2)\times\sum_{n=1}^{\infty}\left[\frac{(Bi^2+\beta_n^2)\cos\beta_n\xi}{\beta_n^2(Bi^2+Bi+\beta_n^2)}\times\sum_{m=1}^{k}\left(\mathrm{e}^{\beta_n^2\left(\frac{m+\delta-1}{f}-\tau\right)}-\mathrm{e}^{\beta_n^2\left(\frac{m-1}{f}-\tau\right)}\right)\right]\right\} \tag{24}$$

where $k \leqslant f\tau - \delta + 1$. Substituting $\xi = 0$ into Eq. (24), the front surface temperature evolution of the slab is

$$\lambda_{\mathrm{s}}(0,\tau) = 2\Theta j_{\mathrm{iw}}\left\{\Delta_1\times\sum_{n=1}^{\infty}\frac{Bi^2+\beta_n^2}{\beta_n^2(Bi^2+Bi+\beta_n^2)}\times(1-\mathrm{e}^{-\beta_n^2\tau}) + (\chi_{\mathrm{bias}}-\Delta_2)\times\sum_{n=1}^{\infty}\left[\frac{Bi^2+\beta_n^2}{\beta_n^2(Bi^2+Bi+\beta_n^2)}\times\sum_{m=1}^{k}\left(\mathrm{e}^{\beta_n^2\left(\frac{m+\delta-1}{f}-\tau\right)}-\mathrm{e}^{\beta_n^2\left(\frac{m-1}{f}-\tau\right)}\right)\right]\right\} \tag{25}$$

If we consider the front surface temperature of the slab solely due to the pulse-on duration, the front surface temperature evolution can be expressed as

$$\lambda_{\mathrm{s}}(0,\tau) = 2\Theta j_{\mathrm{iw}}\left\{(\Delta_1+\chi_{\mathrm{bias}}-\Delta_2)\times\sum_{n=1}^{\infty}\left[\frac{Bi^2+\beta_n^2}{\beta_n^2(Bi^2+Bi+\beta_n^2)}\times\sum_{m=1}^{k}\left(\mathrm{e}^{\beta_n^2\left(\frac{m+\delta-1}{f}-\tau\right)}-\mathrm{e}^{\beta_n^2\left(\frac{m-1}{f}-\tau\right)}\right)\right]\right\} \tag{26}$$

2.3. Plasma heating of a semi-infinite target

The one-dimensional, unsteady heat conduction equation, initial and front boundary conditions in dimensionless forms for the semi-infinite target are similar as Eqs. (9)–(11), respectively. The bottom boundary condition is

$$\lambda_{\mathrm{t}}(\infty,\tau) = 0 \tag{27}$$

The subscript t denotes the semi-infinite target. Eq. (14) can be rewritten as

$$\tilde{\lambda}_{\mathrm{t}}(\xi,s) = \frac{1}{2}\left[\tilde{\lambda}_{\mathrm{t}}(0,s) - \Theta\frac{\mathrm{Q(s)}}{\sqrt{s}}\right]\mathrm{e}^{\sqrt{s}\xi} + \frac{1}{2}\left[\tilde{\lambda}_{\mathrm{t}}(0,s) + \Theta\frac{Q(s)}{\sqrt{s}}\right]\mathrm{e}^{-\sqrt{s}\xi} \tag{28}$$

Applying the boundary condition of the Eq. (27) to Eq. (28), the sum of the coefficients of $\mathrm{e}^{\sqrt{s}\xi}$ must be set equal to zero. The $\tilde{\lambda}_{\mathrm{t}}(0,s)$ is found as

$$\tilde{\lambda}_{\mathrm{t}}(0,s) = \Theta\frac{Q(s)}{\sqrt{s}} \tag{29}$$

Substituting the quantity back into Eq. (28), yields

$$\tilde{\lambda}_{\mathrm{t}}(\xi,s) = \Theta\frac{Q(s)}{\sqrt{s}}\mathrm{e}^{-\sqrt{s}\xi} \tag{30}$$

The inverse Laplace transform is given by

$$L^{-1}\left\{\frac{\mathrm{e}^{-\sqrt{s}\xi}}{\sqrt{s}}\right\} = \frac{\mathrm{e}^{-\frac{\xi^2}{4\tau}}}{\sqrt{\pi\tau}} \tag{31}$$

The inverse Laplace transform of the Eq. (30) can be expressed as

$$\lambda_t(\xi,\tau)=\frac{\Theta j_{iw}}{\sqrt{\pi}}\left\{\Delta_1\times\left[2\sqrt{\tau}e^{-\frac{\xi^2}{4\tau}}-\xi\sqrt{\pi}\times\mathrm{erfc}\left(\frac{\xi}{2\sqrt{\tau}}\right)\right]+(\chi_{bias}-\Delta_2)\times\sum_{n=1}^{k}\left[2\sqrt{\tau-\frac{n-1}{f}}e^{-\frac{\xi^2}{4\left(\tau-\frac{n-1}{f}\right)}}-2\sqrt{\tau-\frac{n+\delta-1}{f}}e^{-\frac{\xi^2}{4\left(\tau-\frac{n+\delta-1}{f}\right)}}-\xi\sqrt{\pi}\left(\mathrm{erf}\left(\frac{\xi}{2\sqrt{\tau-\frac{n+\delta-1}{f}}}\right)-\mathrm{erf}\left(\frac{\xi}{2\sqrt{\tau-\frac{n-1}{f}}}\right)\right)\right]\right\} \tag{32}$$

where $k\leqslant f\tau-\delta+1$. Substituting $\xi=0$ into Eq. (32), the front surface temperature of the semi-infinite target is

$$\lambda_t(0,\tau)=\frac{2\Theta j_{iw}}{\sqrt{\pi}}\left\{\Delta_1\sqrt{\tau}+(\chi_{bias}-\Delta_2)\times\sum_{n=1}^{k}\left[\sqrt{\tau-\frac{n-1}{f}}-\sqrt{\tau-\frac{n+\delta-1}{f}}\right]\right\} \tag{33}$$

Similar as the slab, the front surface temperature of the semi-infinite target solely due to the pulse-on duration can be expressed as

$$\lambda_t(0,\tau)=\frac{2\Theta j_{iw}}{\sqrt{\pi}}\left\{(\Delta_1+\chi_{bias}-\Delta_2)\times\sum_{n=1}^{k}\left[\sqrt{\tau-\frac{n-1}{f}}-\sqrt{\tau-\frac{n+\delta-1}{f}}\right]\right\} \tag{34}$$

The first terms on the right hand side of Eqs. (24) and (32) represent the temperature distributions in the slab and target, respectively, when the bias voltage is zero, $\chi_{bias}=0$. The critical times, τ_m, required to initiate melting on the front surfaces of the slab and target are determined when $\lambda_s(0,\tau)$ and $\lambda_t(0,\tau)$ are identical to λ_m. The effects of pulse parameters on the critical time for onset of melting at the front surface of the slab and target are determined from Eqs. (25) and (33).

3. Results and discussion

To confirm relevancy and accuracy of this model, a comparison between the predicted and measured surface temperatures as a function of time [17] for a hydrogen plasma and silicon wafer are shown in Fig. 2. In this case, the referenced data for comparison are listed in Table 1. The predicted temperature as a function of time agrees quite well with experimental data [17]. The effects of pulse duty cycle and pulse bias voltage on dimensionless temperature evolutions at the front surfaces of the slab and semi-infinite target are shown in Fig. 3. The solid lines (and following figures) are the predicted results based on the

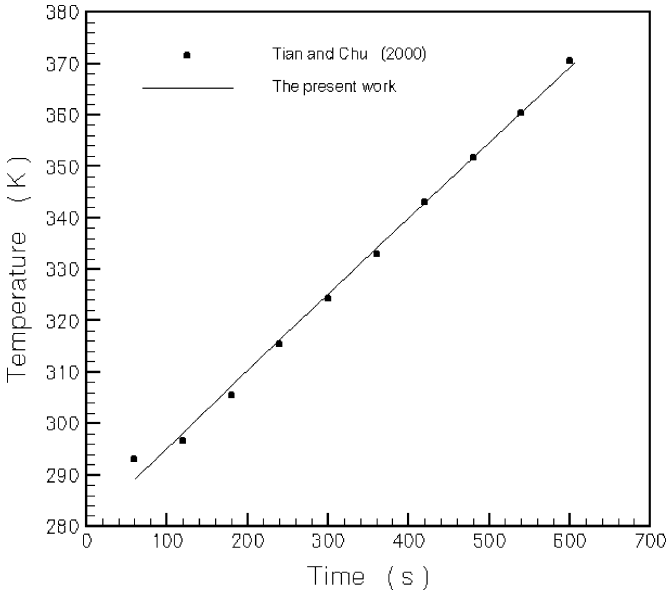

Fig. 2. A comparison of the predicted dimensional temperature at the front surface of a slab versus dimensional time between this work and the results from Tian and Chu [17].

Table 1
Values of the data (hydrogen plasma, silicon slab) for comparison with experimental data [17]

γ	0
γ_e	0
M	1836
Z_i	1
κ	0.1
ϕ_{bias}	−30 kV
t_{on}	30 μs
f	330 Hz
c_p	703 J/kg K
T_0, T_∞	280 K
k	149 W/m K
ρ	2330 kg/m^3
h_∞	1.49 W/m^2 K
S	0.01 m
n_{e0}	2×10^{15} m^{-3}
m_i	1.67×10^{-27} kg
T_{e0}	1×10^4 K
E_i	13.6 eV
φ	4 eV

reference dimensionless parameters from Table 2, which being estimated from the chosen data are $\gamma=0$, $\gamma_e=0$, $M=1836$, $Z_i=1$, $\kappa=0.1$, $\phi_{bias}=-17$ kV, $t_{on}=1$ ms, $f=100$ Hz, $c_p=700$ J/kg K, $T_0=T_\infty=280$ K, $k=150$ W/m K, $\rho=2300$ kg/m^3, $h_\infty=75$ W/m^2 K, $s=0.01$ m, $n_{e0}=2.4\times10^{15}$ m^{-3}, $m_i=1.67\times10^{-27}$ kg, $T_{e0}=2\times10^4$ K, $E_i=13.6$ eV and $\varphi=8$ eV. The various lines shown specify different values of dimensionless parameters, and indicate that these parameters are different from those of the reference parameters. In the referenced case, it can be seen that the dimensionless temperature evolutions at the front surfaces of the slab and target rapidly raise at the earlier stage then gradually slow until equal to 1.04 and 0.187

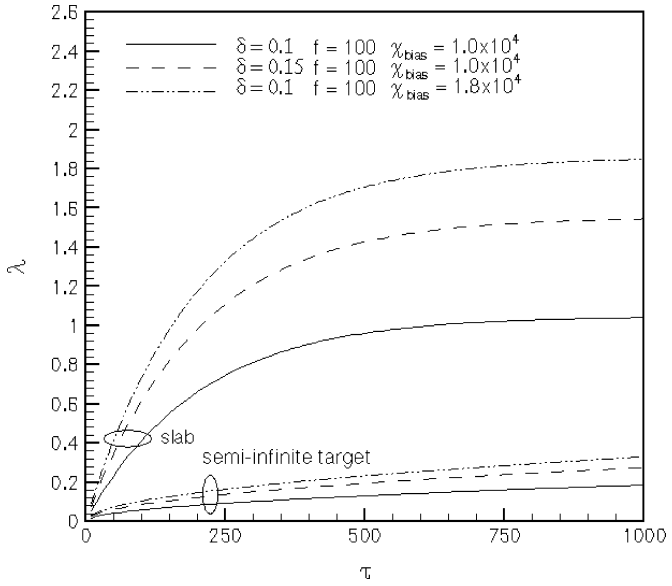

Fig. 3. Dimensionless temperature evolutions at the front surfaces of a slab and semi-infinite target affected by pulse duty cycle and pulse bias voltage; solid lines are based on Table 2.

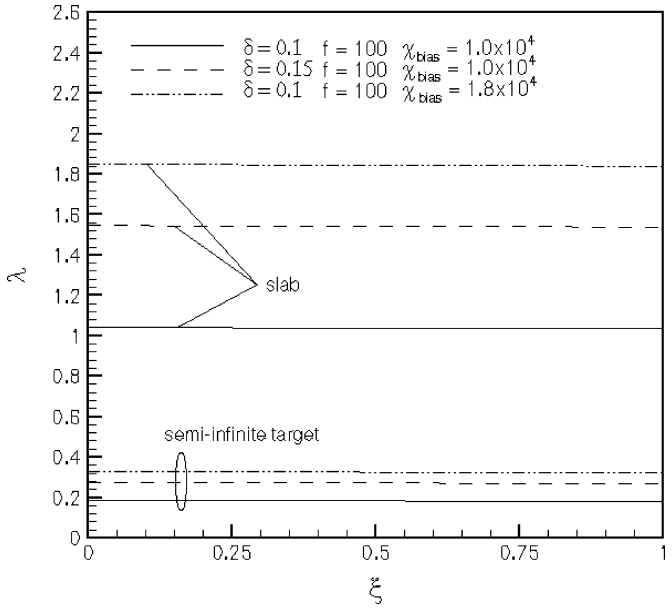

Fig. 4. Variations of dimensionless temperature profiles in the slab and semi-infinite target, the considered depth of semi-infinite target is same as the slab thickness, at $\tau = 1000$ affected by pulse duty cycle and pulse bias voltage; solid lines are based on Table 2.

Table 2
Values of the reference dimensionless parameters

γ	0
γ_e	0
M	1836
Z_i	1
κ	0.1
E_i	8.0
φ	4.6
χ_{bias}	1×10^4
Θ	2×10^{-6}
f	100
δ	0.1
Bi	5×10^{-3}

at $\tau = 1000$, respectively. The surface temperature of the former is about 5.56 times than the latter. An increase in the pulse duty cycle ($\delta = 0.1$–0.15) represents an increase in the dimensionless time for the pulse-on duration, τ_{on}, for constant pulse frequency or an increase in pulse frequency for constant τ_{on} and a decrease in τ_{off}. The surface temperatures of the slab and target increase because the energy incident on the workpiece surface increases with the pulse duty cycle. The higher of pulse bias voltage, the more the ions gain kinetic energy across the sheath. Hence, an increase in pulse bias voltage ($\chi_{bias} = 1 \times 10^4$–$1.8 \times 10^4$), the ions heating the workpiece surface is strong and the surface temperature increases.

The effects of above-mentioned parameters on dimensionless temperature profiles in the slab and target at the dimensionless time $\tau = 1000$ are presented in Figs. 4 and 5. Considering the same dimensionless thickness ($\xi = 1$), the temperature distributions in the slab and target are uniform at $\tau = 1000$ that are shown in Fig. 4. Fig. 5 shows that the temperature profiles in the semi-infinite target vary with

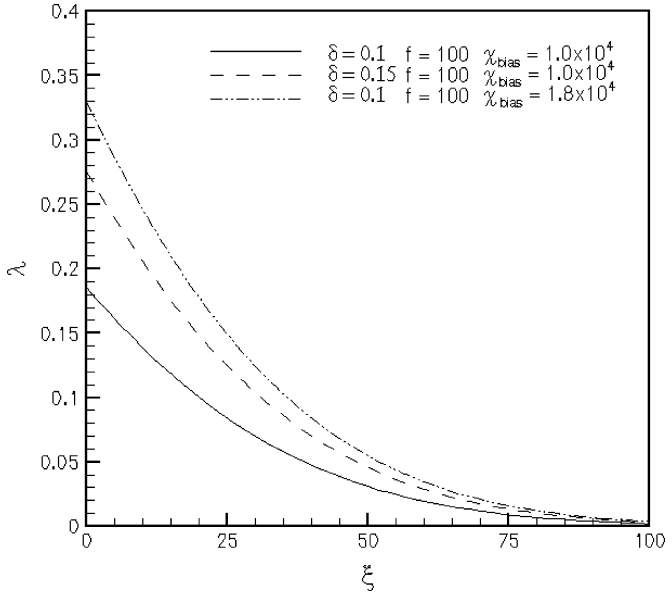

Fig. 5. Variations of dimensionless temperature profiles in the semi-infinite target at $\tau = 1000$ affected by pulse duty cycle and pulse bias voltage; solid lines are based on Table 2.

changing pulse parameters as the thickness of the target is 100 times than the slab. The temperature gradient at the front surface is high and then reduces toward the depth direction. An increase in pulse parameters result in increasing the temperature gradient in the target for the considered thickness.

It is interesting to observe that the pulse bias voltage contributes to the front surface temperature of the workpiece. Therefore, we define a parameter, named pulse

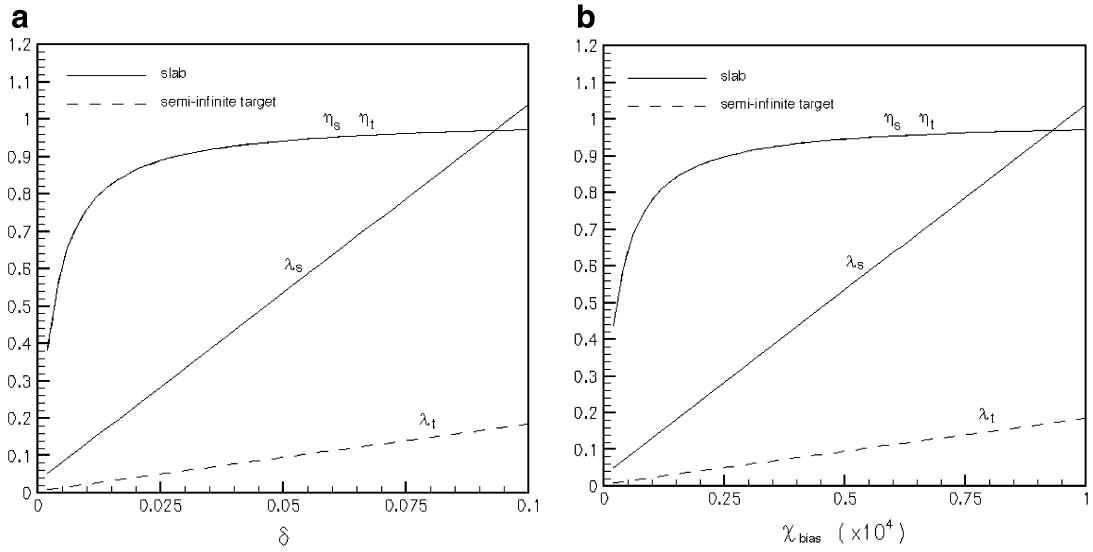

Fig. 6. Dimensionless temperatures at the front surface and pulse efficiency ($\eta = \lambda_{on}/\lambda$) of the slab and semi-infinite target at $\tau = 1000$ affected by: (a) pulse duty cycle and (b) pulse bias voltage.

efficiency, ($\eta = \lambda_{on}/\lambda$, $\lambda = \lambda_{on} + \lambda_{off}$, λ_{on} and λ_{off} denote the front surface temperatures solely due to the pulse-on and pulse-off durations during a pulse cycle, respectively), the temperature at the front surface of the workpiece solely due to pulse-on duration divides by the temperature which includes the effects of pulse-on and pulse-off durations. Fig. 6(a) and (b) shows that the pulse efficiency, and the front surface temperatures of the slab and target vary with different pulse duty cycle and pulse bias voltage, respectively. $\eta_s = \lambda_{s,on}/\lambda_s$ and $\eta_t = \lambda_{t,on}/\lambda_t$ denote the pulse efficiency of the slab and target, respectively. It can be seen that the pulse efficiency of the slab is identical to it of the target for different pulse duty cycle and pulse bias voltage. Because the pulse efficiency is dependent on the energy flux incident on the workpiece surface during the pulse-on and pulse-off durations and the thermophysical properties of the slab and target are same in this work. Therefore, the pulse efficiency of the slab is identical to it of the target for given dimensionless time, pulse duty cycle and pulse bias voltage. The pulse efficiency of the slab and target rapidly increase from about 0.38 to 0.9 for $\delta = 0.002$–0.028, and 0.44–0.9 for $\chi_{bias} = 2 \times 10^2$–$2.6 \times 10^3$, and those approximate constants for $\delta > 0.06$ and $\chi_{bias} > 6 \times 10^3$, respectively. This is because that an increase in pulse duty cycle results in an increase in λ_{on} and a decrease in λ_{off}. On the other hand, an increase in pulse bias voltage results in an increase in λ_{on} and has no influence on λ_{off}. It is obvious that the heating of plasma on the workpiece due to self-bias is important during pulse-off duration for low pulse duty cycle and low pulse bias voltage. The pulse efficiency and front surface temperature of the slab is around $\eta_s = 0.38$ and $\lambda_s = 0.05$ for $\delta = 0.002$ and $\chi_{bias} = 1 \times 10^4$, respectively, as shown in Fig. 6(a). The corresponding front surface temperature due to pulse-on and pulse-off durations are around $\lambda_{s,on} = 0.02$ and $\lambda_{s,off} = 0.03$, respectively. Another, the pulse efficiency and front surface temperature of the slab is around $\eta_s = 0.44$ and $\lambda_s = 0.05$ for $\delta = 0.1$ and $\chi_{bias} = 2 \times 10^2$, respectively, as shown in Fig. 6(b). The corresponding front surface temperature due to pulse-on and pulse-off durations are around $\lambda_{s,on} = 0.02$ and $\lambda_{s,off} = 0.03$, respectively. The effects of the pulse-off duration on the front surface temperature of the workpiece is larger than that during pulse-on duration for low pulse duty cycle and low pulse bias voltage. This is because that the lower the pulse duty cycle (pulse bias voltage), the less the energy flux transport to the workpiece surface during pulse-on duration. The front surface temperatures of the slab and target almost linearly increase with different pulse parameters. The front surface temperature ratios of the slab-to-target is about 5.5 for different pulse parameters.

Dimensionless melting time at the front surface of a slab and a semi-infinite target as function of pulse duty cycle and pulse bias voltage are shown in Fig. 7(a) and (b), respectively. In these figures, the solid and dashed lines correspond to the slab and target, respectively. The melting times are calculated based on the dimensionless temperature of the workpiece surface reach $\lambda_m = 1$. An increase in pulse duty cycle and pulse bias voltage represent an increase in the time of pulse-on duration per pulse cycle or an increase in pulse frequency for the constant pulse-on duration and the kinetic energy of incident ions per pulse cycle, respectively. Therefore, the incident energy transport to the workpiece surface increases and the surface temperature raises. In Fig. 7(a) and (b), the melting times of the slab and target rapidly drop then gradually decrease from 617 to 23, 20 and 2.8×10^4–3.8×10^2, 3×10^2 for $\delta = 0.1$–0.9 and $\chi_{bias} = 1 \times 10^4$–$1 \times 10^5$, respectively. The results show that the time to initiate the melting at the front surface of the target is longer than the slab for the same processing conditions.

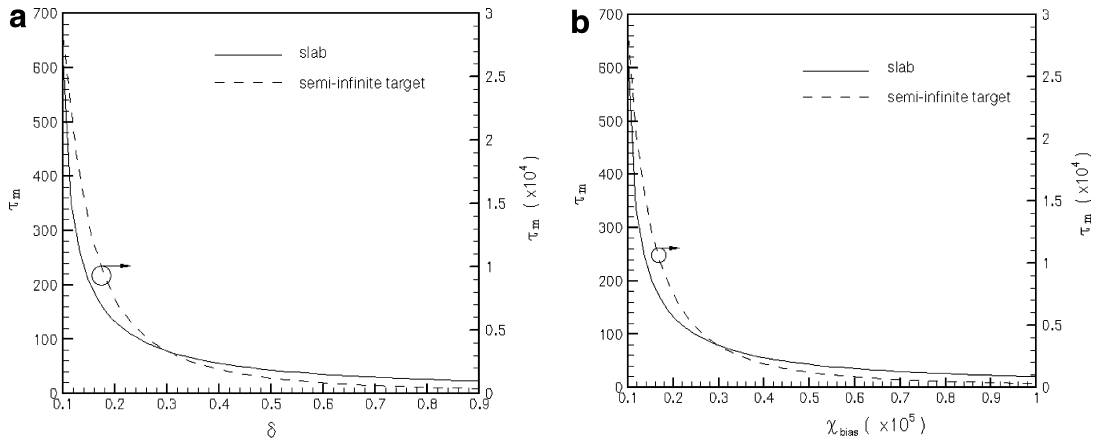

Fig. 7. Dimensionless melting times at the front surfaces of a slab and semi-infinite target for $\lambda_m = 1$ affected by (a) pulse duty cycle and (b) pulse bias voltage.

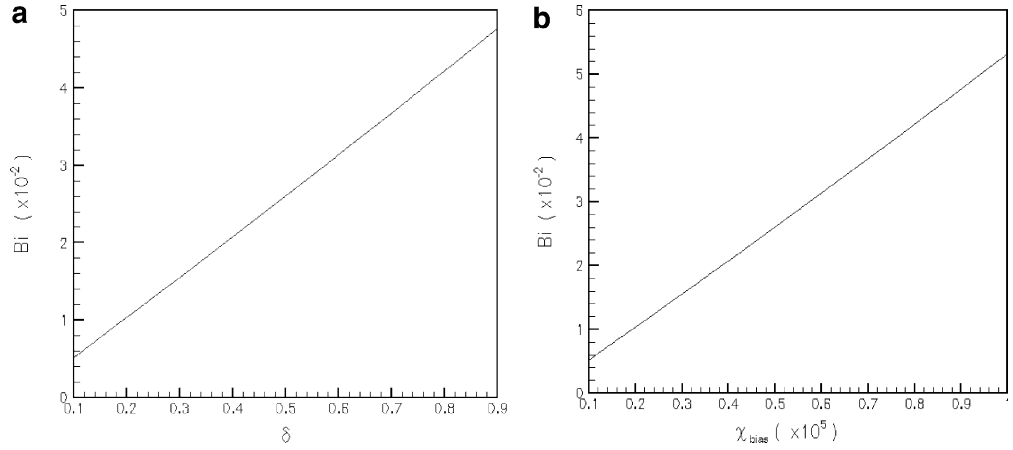

Fig. 8. Biot numbers for avoid initiating the melting of front surface of a slab for $\lambda_m = 1$ and $\tau = 1000$ affected by (a) pulse duty cycle and (b) pulse bias voltage.

The higher the Biot number, the quicker the heat is removed by convection to the surroundings. The front surface temperature of the slab is deeply affected by the Biot number at the bottom of the slab. Because the energy flux incident on the slab surface increases with pulse duty cycle and pulse bias voltage, it is important to determine the Biot number for different pulse parameters to avoid initiating the melting at the front surface of the slab. Fig. 8(a) and (b) shows that the front surface temperature of slab reaches the melting temperature $\lambda_m = 1$ at $\tau = 1000$, the Biot number vary with pulse parameters. The front surface temperature of the slab linearly increase with pulse parameters, and the temperature distribution in the slab is uniform that can be found from Figs. 6(a), (b) and 4, respectively. According to the above description, the rear surface temperature also linearly increase with pulse parameters that results in the Biot number increases with the pulse parameters. The Biot number increase from 0.5 to 4.8 and 0.5 to 5.3 for $\delta = 0.1$–0.9 and $\chi_{bias} = 1 \times 10^4$–$1 \times 10^5$, respectively.

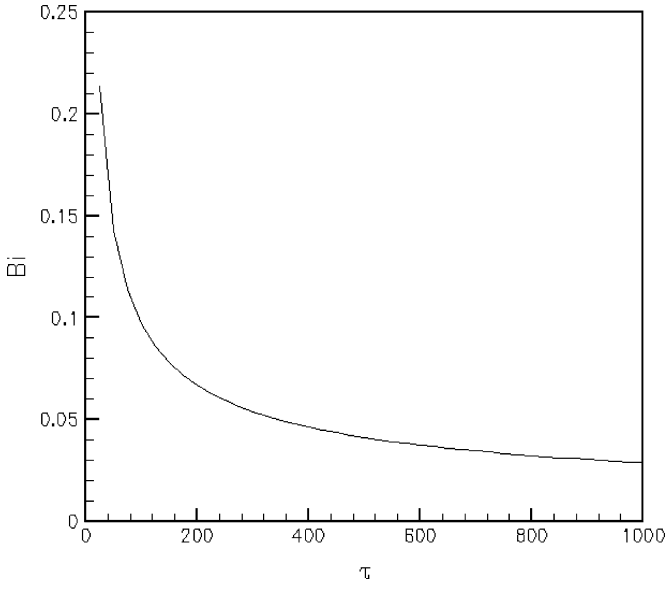

Fig. 9. Variations of Biot number versus dimensionless time for the front surface temperatures of a slab and semi-infinite target are identical.

It is interested that the front surface temperature of the target is simulated with the slab by changing the Biot number. Fig. 9 presents the variation of Biot number with dimensionless time while the front surface temperatures of slab and target are identical. It can be seen from Fig. 3 that the heating rate and temperature of the front surface of the slab is higher than those of the target at the earlier time. In order to reduce the front surface temperature of the slab equal to the target, the Biot number is large at the earlier time. As the time proceeding, the Biot number rapidly drops and gradually reduce to constant. The corresponding Biot number is 0.214 and 0.029 for $\tau = 25$ and $\tau = 1000$, respectively. The former is about seven times than the latter.

4. Conclusions

1. Plasma heating of workpieces is important for plasma immersion ion implantation. It is crucial to control the temperature of the workpieces to improve the ion diffusion rate in ion implantation process. Semi-analytical solutions are derived by using the two-dimensional Laplace integral transform technique to calculate the temperature evolutions and the melting times of the front surfaces of a slab and semi-infinite target with repetitive high negative bias voltage pulses in contact with a plasma. This work provides quantitative results applicable to control the temperature evolutions and the melting times of the slab and semi-infinite target. The effects of pulse parameters on the temperature evolutions and melting times of the slab and target are found to be significant. The predicted surface temperature evolution of the slab agrees well with experimental data. The results can be used to control the temperature evolutions and the melting times of those by choosing appropriate process parameters.
2. The temperatures and heating rates of the front surface of the slab and semi-infinite target increase with pulse duty cycle and pulse bias voltage so that the melting times to initiate the melting at the front surface of the workpiece reduce. The heat flux transport to workpiece from plasma is important to increase the surface temperature of the workpiece when the bias voltage is switched-off for low pulse duty cycle and low pulse bias voltage. The temperature of the workpiece is underestimated when not accounting for the heating effects during the pulse-off duration for low value of pulse parameters.

References

[1] P.K. Chu, Recent developments and applications of plasma immersion ion implantation, J. Vac. Sci. Technol. B 22 (1) (2004) 289–296.
[2] J.R. Conrad, J.L. Radtke, R.A. Dodd, F.J. Worzala, N.C. Tran, Plasma source ion-implantation technique for surface modification of materials, J. Appl. Phys. 62 (11) (1987) 4591–4596.
[3] J.R. Conrad, Sheath thickness and potential profiles of ion-matrix sheaths for cylindrical and spherical electrodes, J. Appl. Phys. 62 (3) (1987) 777–779.
[4] P.S. Wei, F.B. Yeh, C.Y. Ho, Distribution functions of positive ions and electrons in a plasma near a surface, IEEE Trans. Plasma Sci. 28 (4) (2000) 1244–1253.
[5] P.S. Wei, F.B. Yeh, Fluid like transport variables in a kinetic, collisionless plasma near a surface with ion and electron reflections, IEEE Trans. Plasma Sci. 28 (4) (2000) 1233–1243.
[6] M.A. Lieberman, Model of plasma immersion ion implantation, J. Appl. Phys. 66 (7) (1989) 2926–2929.
[7] J.T. Scheuer, M. Shamim, J.R. Conrad, Model of plasma source ion implantation in planar, cylindrical, and spherical geometries, J. Appl. Phys. 67 (3) (1990) 1241–1245.
[8] B.P. Wood, Displacement current and multiple pulse effects in plasma source ion implantation, J. Appl. Phys. 73 (10) (1993) 4770–4778.
[9] S. Mändl, R. Günzel, W. Möller, Sheath and presheath dynamics in plasma immersion ion implantation, J. Phys. D: Appl. Phys. 31 (1998) 1109–1117.
[10] K.-U. Riemann, Th. Daube, Analytical model of the relaxation of a collisionless ion matrix sheath, J. Appl. Phys. 86 (3) (1999) 1202–1207.
[11] A. Anders, Fundamentals of pulsed plasma for materials processing, Surf. Coat. Technol. 183 (2004) 301–311.
[12] G.A. Emmert, Model for expanding sheaths and surface charging at dielectric surfaces during plasma source ion implantation, J. Vac. Sci. Technol. B 12 (2) (1994) 880–883.
[13] M.P. Hong, G.A. Emmert, Two-dimensional fluid modeling of time-dependent plasma sheath, J. Vac. Sci. Technol. B 12 (2) (1994) 889–896.
[14] T.E. Sheridan, Ion focusing by an expanding, two-dimensional plasma sheath, Appl. Phys. Lett. 68 (14) (1996) 1918–1920.
[15] M.J. Goeckner, R.P. Fetherston, W.N.G. Hitchon, N.C. Horswill, E.R. Keiter, M.M. Shamim, R.A. Breun, J.R. Conrad, T.E. Sheridan, Dynamics of collisional pulsed planar sheaths, Phys. Rev. E 51 (4) (1995) 3760–3763.
[16] R.A. Stewart, M.A. Lieberman, Model of plasma immersion ion implantation for voltage pulse with finite rise and fall times, J. Appl. Phys. 70 (7) (1991) 3481–3487.
[17] X. Tian, P.K. Chu, Direct temperature monitoring for semiconductors in plasma immersion ion implantation, Rev. Sci. Instrum. 71 (7) (2000) 2839–2842.
[18] X. Tian, Z. Fan, X. Zeng, Z. Zeng, B. Tang, P.K. Chu, In situ sample temperature measurement in plasma immersion ion implantation, Rev. Sci. Instrum. 70 (6) (1999) 2818–2821.
[19] X. Tian, P.K. Chu, Target temperature simulation during fast-pulsing plasma immersion ion implantation, J. Phys. D: Appl. Phys. 34 (2001) 1639–1645.
[20] K. Takaki, D. Koseki, T. Fujiwara, Determination of heat and ion fluxes in plasma immersion ion implantation by in situ measurement of temperature using laser interferometry, Surf. Coat. Technol. 136 (2001) 261–264.
[21] A. Mitsuo, S. Uchida, T. Aizawa, Effects of pulse bias voltage and nitrogen pressure on nitrogen distribution in steel substrate by plasma immersion ion implantation of nitrogen, Surf. Coat. Technol. 186 (2004) 196–199.
[22] J.P. Blanchard, Target temperature prediction for plasma source ion implantation, J. Vac. Sci. Technol. B 12 (2) (1994) 910–917.
[23] D. Manova, S. Mändl, B. Rauschenbach, Heat balance during plasma immersion ion implantation, plasma sources, Sci. Technol. 10 (2001) 423–429.
[24] F.B. Yeh, P.S. Wei, Plasma energy transport to an electrically biased surface, Int. J. Heat Mass Transfer 47 (2004) 4019–4029.